Transformation of Fe-P complexes in bioreactors and P recovery from sludge: Investigation by XANES spectroscopy and DFT calculation

Ruo-hong Li[†], Jin-li Cui[§,⊥], Jia-hui Hu[†], Wei-jun Wang[†], Bing Li[†],

Xiang-dong Li[§], Xiao-yan Li[*,†,‡,‖]

[†]Shenzhen Engineering Research Laboratory for Sludge and Food Waste Treatment and Resource Recovery, Graduate School at Shenzhen, Tsinghua University, Shenzhen, China

[‡]Environmental Engineering Research Centre, Department of Civil Engineering, The University of Hong Kong, Pokfulam, Hong Kong, China

[§]Department of Civil and Environmental Engineering, The Hong Kong Polytechnic University, Hung Hom, Kowloon, Hong Kong, China

[‖]Tsinghua-Berkeley Shenzhen Institute, Tsinghua University, Shenzhen, China

[⊥]Key Laboratory for Water Quality and Conservation of the Pearl River Delta, Ministry of Education; School of Environmental Science and Engineering, Guangzhou University, Guangzhou, China

(*Corresponding author: phone: 852-28592659; fax: 852-28595337; E-mail: xlia@hku.hk)

Abstract

The transformation of Fe-P complexes in bioreactors can be important for phosphorus (P) recovery from sludge. In this research, X-ray absorption near edge structure (XANES) analysis was conducted to quantify the transformation of Fe and P species in the sludge of different aging periods and in the subsequent acidogenic sludge co-fermentation for P recovery. Density functional theory (DFT) was applied to analyze the intermediates during the transformation of the identified Fe and P species. P was readily removed from wastewater by Fe-facilitated chemical precipitation, and could be extracted and recovered from sludge via acidogenic co-

fermentation with food waste. Fresh Fe-P-containing sludge was more favorable than aged sludge for Fe-P mobilization and dissolution via acidogenic fermentation and microbial iron reduction. The DFT results indicated that ferric iron dosed into wastewater underwent rapid hydrolysis, clustering, aggregation, and slow crystallization to form hydrous iron oxides (HFO) with various complicated structures. The fresh Fe-based sludge mainly contained fresh ferrihydrite and amorphous $FePO_4$ with sufficient accessible surface area for microbial reaction. With the aging of sludge in bioreactors, the HFO densified into crystal phases (e.g., goethite) with much reduced surface area and reactivity, which greatly increased the difficulty of P recovery. Thus, aging of P-containing sludge should be minimized in wastewater treatment systems for the purpose of P recovery.

Table of Contents (TOC)

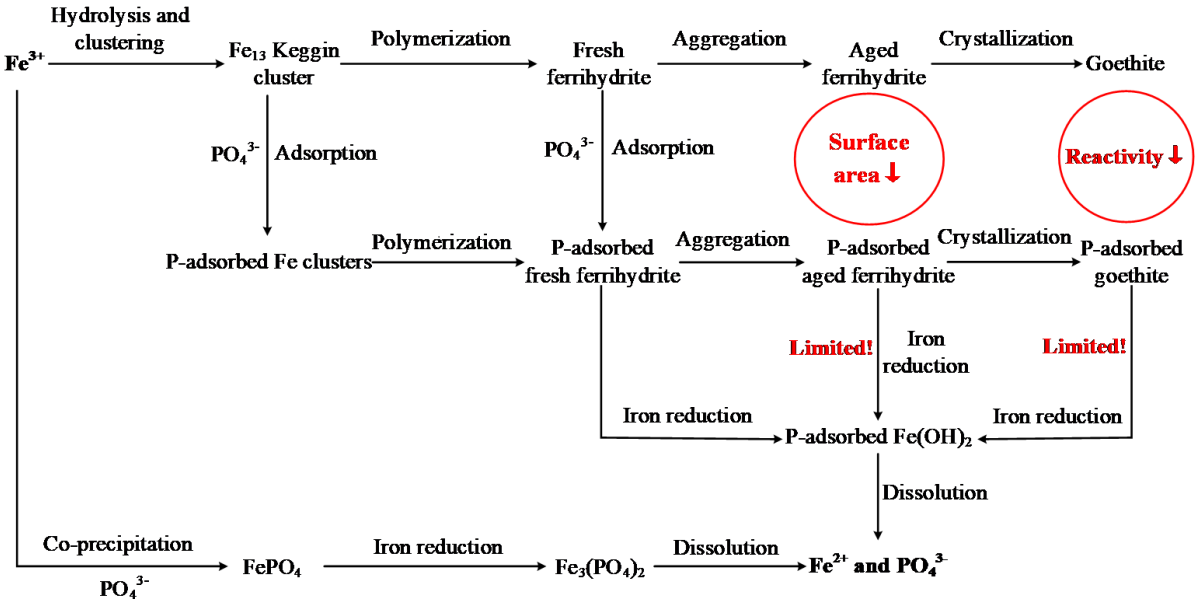

1. Introduction

Phosphorus (P) is a limited a resource related to food security. With the rapid consumption of natural phosphate rock, the crisis of P depletion has been predicted to happen before the end

of this century.[1] Sustainable utilization and recovery of P resources are urgently needed. Every year, around 1.3 million tons of P pass through wastewater treatment plants (WWTPs) globally. Recovery of P from wastewater streams would satisfy an estimated 15-20% of the global P demand and considerably alleviate the P crisis.[1] P is known as an important nutrient pollutant in wastewater discharge. To meet the stringent discharge limit (<0.2 mg/L in China[2]), WWTPs commonly apply the chemical P removal (CPR) method, which involves dosing metal salts into wastewater to precipitate and remove phosphate from the liquid phase. $FeCl_3$ is an efficient chemical flocculant for such an application. For instance, $FeCl_3$ has been dosed into membrane bioreactors (MBRs) to improve the P removal efficiency.[3] With this Fe-facilitated chemical treatment, the effluent P concentration can be reduced to as low as 0.1 mg/L,[4, 5] and most of the residual P is concentrated in the Fe-based sludge. It is desirable to recover the residual P from this Fe-based P-containing sludge. In fact, the recently approved German Sewage Sludge Ordinance legally requires P recovery from sewage sludge in all German WWTPs of larger than 50,000 person equivalents.[6]

Chemical acidification extraction is a commercial method of extracting P from chemically enhanced sludge, which however is expensive and causes secondary pollution.[7] Enhanced biological phosphorus removal (EBPR) combined with anaerobic sludge digestion is another strategy for both P removal and recovery in wastewater treatment. However, the startup of the EBPR process can be difficult as it requires stringent operating conditions and often suffers from poor stability in operation.[8] In recent studies, an acidogenic P recovery (APR) method has been developed, in combination with the CPR process, to achieve effective and environmentally friendly P recovery in wastewater treatment.[9] The process utilizes the different solubility of ferric and ferrous compounds, transforming the former to the more soluble latter through biological dissimilatory iron reduction via acidogenic sludge fermentation. The resulting Fe^{II}-P complexes are more easily dissolved, releasing P into the liquid phase of the

sludge for potential recovery. The overall efficiency of P recovery from wastewater by the CPR-APR process can reach as high as 60%.

However, the transformation of Fe-P complexes in wastewater treatment systems is complex, and its influence on P recovery has not been fully understood. The long retention time of Fe-P sludge in aerobic bioreactors makes Fe-P complexes more complicated, affecting their solubility during sludge fermentation for P extraction and recovery. Bacteria, such as iron-oxidizing bacteria (IOB) and iron-reducing bacteria (IRB), can utilize Fe as an electron donor or acceptor in metabolic activities. The interactive biological and chemical reactions in the aqueous and solid phases in relation to the transformation of Fe and P species have not been well addressed. The effect of the aging process of Fe-based sludge in bioreactors on the efficiency of P recovery from the sludge by the subsequent APR has also not been investigated.

The chemistry of iron with P is very diverse.[10-12] As a transition metal, the valence state of iron (Fe) can vary from -2 to +6, whilst +2 (Fe^{II}) and +3 (Fe^{III}) are the most common states. The hydrous form of Fe^{III} can form various insoluble chemicals, termed hydrous iron oxides (HFO), including ferrihydrite, goethite, akaganeite, and lepidocrocite.[10] In wastewater treatment, the Fe-P complexes are usually found in either $FePO_4$-containing minerals or in the form of P adsorbed onto HFO.[13] The transformation of HFO structures alters their behavior in both biological and chemical reactions. Georgaki et al.[14] found that the acid leaching reactivity of Fe-rich sludge decreased as the sludge aged due to increases in particle size and/or degree of crystallinity. Bonneville et al.[15] conducted experiments on microbial iron reduction of different crystalline iron oxides by the *Shewanella alga* strain BrY and found that amorphous iron oxides with a higher surface area were more favorable for IRB growth and iron reduction. However, the mechanisms of Fe-P complex formation and their further transition and aging in sludge in relation to P recovery in APR bioreactors are urgently required.

In this study, the transformations of Fe and P species in Fe-P-containing sludge after

different retention periods in aerobic bioreactors were fully investigated, as well as their effect on P extraction from the sludge during the APR process. A powerful characterization technique, X-ray absorption spectroscopy (XAS), was implemented for Fe and P species analysis, which is known to be able to quantify species compositions in sludge.[13] Based on the X-ray absorption near edge structure (XANES) analysis, the Fe and P species in the sludge after different retention periods, and the corresponding transformations during the acidogenic fermentation process, were revealed in details. As the intermediates during the Fe and P transformation are difficult to be detected directly, a computational method was further applied to analyze the possible intermediate forms between the Fe-related compounds identified from the XANES results. The findings on the transformations of Fe and P in sludge after different aging periods provide new insights into the pathways and controlling factors for effective P removal and recovery in chemical-biological wastewater treatment systems.

2. Materials and Methods

2.1 Retention and aging of Fe-P precipitate-containing sludge in bioreactors

Raw municipal wastewater was collected from Nanshan Wastewater Treatment Plant in Shenzhen, China. The wastewater had a chemical oxygen demand (COD) concentration of around 150 mg/L, a total phosphorus (TP) concentration of around 5 mg/L, and a total nitrogen (TN) concentration of around 21 mg/L. Seed-activated sludge was also obtained from the aerobic tank in the same wastewater treatment plant.

Fe-P-containing sludge was prepared from the wastewater by the CPR method. As a chemical coagulant, $FeCl_3$ (15 mg-Fe/L) was dosed into the raw wastewater for rapid mixing (200 rpm) for approximately 5 min in a stirring tank, followed by 15 min of slow mixing and 30 min of sedimentation. The settled sludge was then collected for the subsequent experimental study in the bioreactors.

116 The aging and transformation of the Fe-P complexes in the sludge were investigated in
117 aerobic MBRs. Two MBRs were operated in parallel, each having a working volume of 25 L.
118 The Fe-P sludge was mixed into the activated sludge with a mixed-liquor suspended solids
119 (MLSS) concentration of about 4.9 g/L in the MBRs. Aeration via an air diffuser at the bottom
120 kept the dissolved oxygen (DO) at around 3.0-3.5 mg/L in the MBRs. Synthetic wastewater
121 was supplied as the influent containing 100 mg-COD/L of glucose, 20 mg-N/L of ammonia,
122 and 50 mg/L of $NaHCO_3$. The use of MBRs prevented the loss of Fe-P precipitates from the
123 sludge suspension. The MBRs were operated at a low loading condition with a low sludge yield,
124 and the sludge production was approximately balanced by the sludge sampling from the
125 bioreactors, resulting in little change of the MLSS concentration during the 1-month MBR test.
126 The sludge mixture was sampled from the MBRs after the pre-determined aging periods, i.e.,
127 0, 4, 7, 10, and 30 d, which were equivalent to the solids retention times (SRTs) of the Fe-P
128 sludge in the bioreactors. Before the subsequent test of APR, the sludge samples were analyzed
129 for suspended solids (SS), volatile suspended solids (VSS), and Fe and P species.

130 **2.2 Batch experiment for acidogenic P extraction and recovery from the sludge**

131 The Fe-P-rich sludge from the MBRs was processed by co-fermentation with food waste
132 for P extraction and recovery from the sludge. For the APR, each sludge sample after a certain
133 retention period in the MBRs (i.e., 0, 4, 7, 10, or 30 d) was mixed with food waste in a 500-
134 mL glass bottle as an anaerobic fermenter. The sludge suspension placed in the fermenter
135 contained about 5 g/L of SS, with around 287 mg/L of TP and 833 mg/L of total iron (TFe).
136 Food waste was collected from the school canteen in Shenzhen University Town and crushed
137 into slurry, which was added into the sludge suspensions to have 6 g-COD/L in the fermenters.
138 Under anaerobic conditions, sludge with a rich organic content undergoes acidogenic
139 fermentation.[16] The co-fermentation experiment for each MBR sludge sample was conducted
140 for 6 days in duplicate. During the process, P and Fe were expected to be released from the

141 solid phase into the supernatant of the sludge. The sludge mixture was sampled every day for
142 measurement of pH, SS, VSS, soluble orthophosphate (SP), soluble ferrous iron (SFe^{II}), and
143 volatile fatty acids (VFAs). After the 6-d co-fermentation, the sludge was sampled and
144 centrifuged at 6000 rpm for 15 min and the sludge pellet was retrieved. The sludge pellet was
145 freeze-dried overnight to prepare the powder sample for the XANES analysis. Before the co-
146 fermentation, the activated sludge from the MBRs was also centrifuged to obtain the sludge
147 pellet for the XANES analysis. The dry sludge powder was kept in a glass bottle filled with N_2
148 and stored at -20°C before XANES.

149 **2.3 X-ray absorption near edge structure spectroscopy for P and Fe speciation**

150 The P and Fe speciation in the sludge samples was determined by XAS on beamline 16A1
151 at the National Synchrotron Radiation Research Center (NSRRC), Taiwan. The powder
152 samples and references were pressed into pellets 5 mm in diameter and 1 to 2 mm in thickness,
153 which were immediately pasted on Kapton tape before measurement. The P and Fe species
154 were detected by P K-edge (2145.5 eV) and Fe K-edge (7112.0 eV) radiation, respectively,
155 using a Si(111) double-crystal monochromator. The X-ray energy was calibrated by measuring
156 the L_{III}-edge of Nb foil for P with E_0 at 2153.4 eV and Fe metal foil for Fe with E_0 at 7124.6
157 eV. E_0 was calculated as the maximum peak energy of the 1st derivative of the spectra. The
158 measurement was performed in fluorescence mode using an ionization chamber filled with
159 helium gas (for I_0) and a Lytle detector filled with nitrogen gas (for I_f) under ambient
160 temperature and pressure. The representative Fe and P reference compounds selected for
161 XANES analysis, including amorphous ferric phosphate, strengite, vivianite, phosphate
162 adsorbed on HFO, phytic acid sodium salt hydrate, hydroxyapatite, newberyite, sodium
163 phosphate dibasic, ferrihydrite, goethite, akaganeite, lepidocrocite, siderite, melanterite,
164 ferrous chloride tetrahydrate, pyrite, magnetite, ferric oxide, ferrous oxide, ferric nitrate
165 nonahydrate, ferrous oxalate dihydrate, and ferric citrate, are listed in supporting information

(Figure S1). Details of the chemical suppliers and the references for the synthesis procedures are also provided in the supporting information.

The collected XANES spectra were first processed by principal component analysis (PCA) and target transformation (TT) using the SIXPack code[17, 18] to select appropriate reference compounds possibly existing in the sludge samples. The linear combination fitting (LCF) analysis in the Athena program was further applied to identify and quantify the Fe and P species, as well as their fractions, in the sludge samples.[19]

2.4 Analytical methods

All samples were analyzed in triplicate, and the results obtained are the mean values with standard errors of the measurements. The concentrations of COD, TN, SP, TP, SFe^{II}, TFe, SS, and VSS were measured according to Standard Methods.[20] For determining the concentrations of soluble chemicals, the samples were filtered via a 0.45-μm PVDF membrane (Millipore) and the filtrates were measured. For detection of total Fe^{II} (TFe^{II}) and total Fe^{III} (TFe^{III}) in sludge, 100 mL sludge was diluted to 1000 mL with deionized water and the pH was reduced to below 2 by adding HCl to dissolve all iron species into the liquid phase.[12] The solution was then stirred for 1 h, and the concentrations of TFe^{II} and TFe^{III} in the filtrate were determined. The insoluble Fe^{II} and Fe^{III} can be calculated by subtracting SFe^{II} and SFe^{III} from TFe^{II} and TFe^{III}, accordingly.

The pH was measured by a Starter 2100 pH meter (OHAUS), the dissolved oxygen (DO) concentration was detected by an HI 2030 DO meter (HANNA), and the oxidation-reduction potential (ORP) was measured by an HI 98201 ORP meter (HANNA). Volatile fatty acids (VFAs) were measured by an Agilent 6890 gas chromatograph (GC) with an Agilent 19095F-123 capillary column and a flame ionization detector, following the method described previously.[9]

2.5 Computational

The energies of the Fe-related compounds were calculated using density functional theory (DFT) in the Vienna Ab-initio Simulation Package (VASP).[21] The projector-augmented wave (PAW) method was used to describe electron-ion interactions.[19,20] The generalized gradient approximation (GGA)+U parametrized by the Perdew-Burke-Ernzerhof (PBE) pseudopotential was applied to correct the on-site Coulomb repulsion of 3d electrons of Fe with U_{eff} = 5.30 eV.[22,23] Taking into account the magnetic properties of iron, the magnetizations of Fe^{III} and Fe^{II} were set at 5 and 4, respectively.[24] The cutoff energy was set at 520 eV,[25] and the self-consistent field (SCF) convergence tolerance was 1×10^{-5} eV. A k-point mesh with gamma-centered Monkhorst-Pack grids was used for all structures, which was generated by VASPKIT for VASP.[26]

All of the energies were corrected for Gibbs free energy at 298.15 K and 1 atm. The total energies of H_2O, $Fe(OH)_2$, CH_3COOH, CH_3CH_2COOH, and CO_2 molecules in isolation were calculated in a periodic supercell box of 10×10×10 $Å^3$, [27, 28] while for the Fe_{13} Keggin cluster, a box of 20×20×20 $Å^3$ was used to ensure no intermolecular interactions.

3. Results and Discussion

3.1 Acidogenic P recovery from Fe-enhanced sludge with different ages

Chemically enhanced phosphorus removal is an effective and reliable method to remove P from wastewater. In this study, by dosing $FeCl_3$ into the wastewater, more than 95% of TP was removed and concentrated into the Fe-based sludge. The Fe-P sludge was then mixed with activated sludge in the aerobic MBRs. The TP and TFe concentrations in the sludge mixture were around 287 and 832 mg/L, respectively. After different retention and aging periods in the MBRs, the Fe-P-containing sludge mixtures were collected and fed into the anaerobic bioreactors for 6-d co-fermentation with food waste. During fermentation, the sludge

underwent hydrolysis and acidogenesis, releasing P into the supernatant for potential recovery. The performance of APR from the different sludge samples is shown in Figure 1.

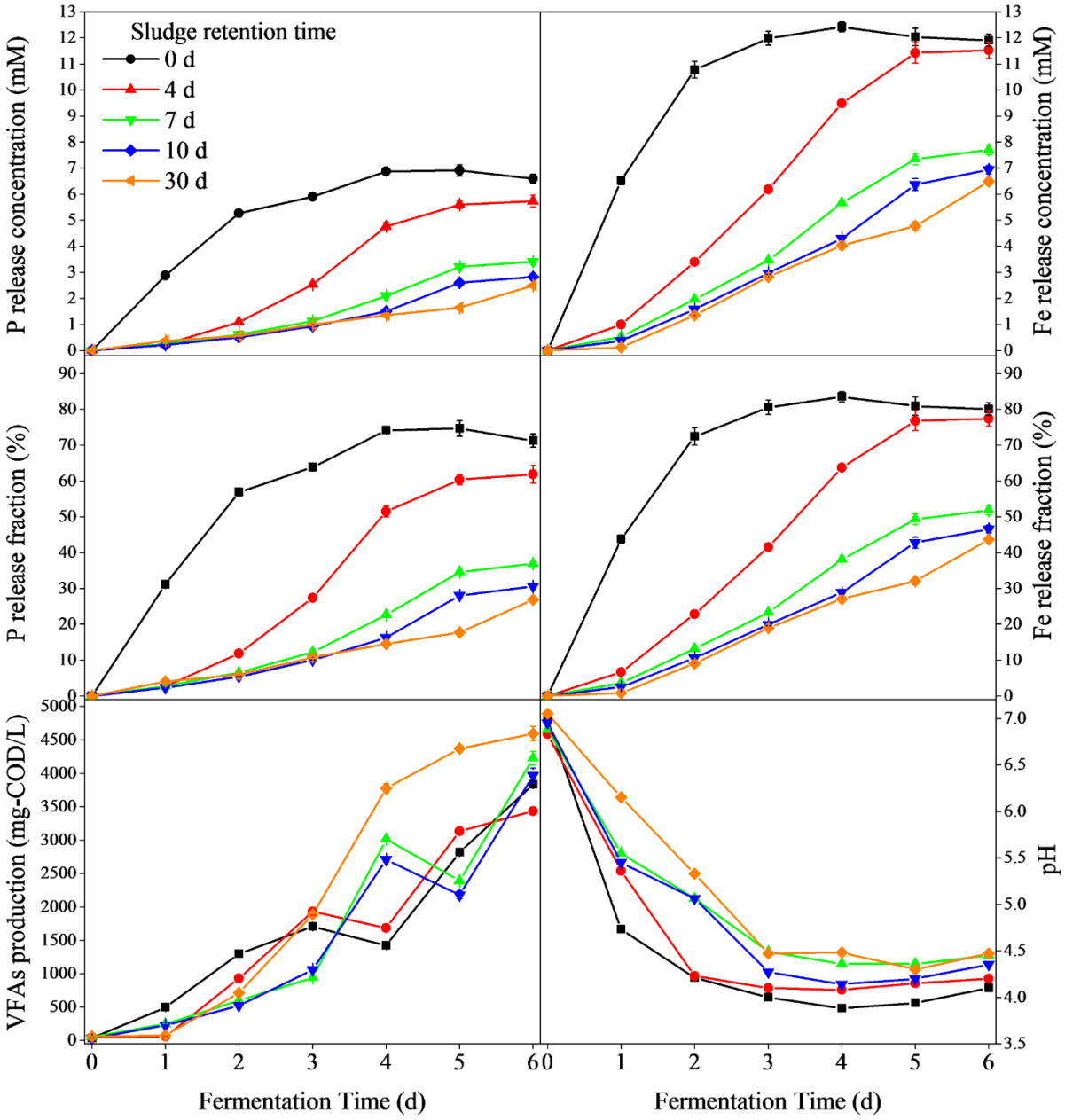

Figure 1. Acidogenic P recovery performance during acidogenic fermentation.

Conventional anaerobic digestion usually consists of three steps: hydrolysis, acidogenesis, and methanogenesis. Acidogenic fermentation can be achieved when methanogenesis is inhibited via appropriate loading, duration, and pH control.[29] Food waste mainly contains easily biodegradable organics, which can be quickly hydrolyzed into soluble organics that are then

converted into VFAs to decrease the solution pH.[30] When the pH is maintained between 4 and 5, methane production can be largely inhibited. As shown in Figure 1, with 6 g-COD/L food waste addition, the VFA concentration continuously increased to around 4 g-COD/L during 6-d fermentation, leading to a significant pH decrease.

During the anaerobic co-fermentation, the ORP of the sludge was reduced to below -100 eV. Under this condition, IRB can utilize soluble organics as electron donors to effectively reduce Fe^{III} to Fe^{II} compounds via microbial dissimilatory iron reduction in the Fe-containing sludge.[31] At low pH (<4.5) and low ORP (<-100 eV), the solubility of Fe^{II} compounds increased, releasing Fe^{2+} and PO_4^{3-} into the supernatant liquid. As shown in Figure 1, for the fresh Fe-containing sludge mixture without aging (SRT = 0 d), the soluble Fe^{II} concentration quickly increased to about 12 mM in the first 4 d, corresponding to 80% of the total Fe in the sludge. Meanwhile, SP was also released and increased in concentration to around 7 mM, accounting for 75.0% of the total P in the sludge. However, for the Fe-containing sludge with longer aging periods (SRTs) of 4, 7, 10, and 30 d, the maximum P release efficiency decreased from 75.0% to 61.9%, 36.9%, 30.6%, and 26.9%, correspondingly. As the retention time of the Fe-based sludge increased in the aerobic bioreactors, the efficiency of APR from the sludge significantly decreased and it took longer fermentation times to reach the maximum P release concentration. The retention of Fe-P complexes in the bioreactors evidently led to considerable transformations of the Fe and P species, making it difficult to solubilize the Fe-P complexes. Thus, it is necessary to investigate the Fe and P transformations during the retention of sludge in the bioreactors and understand how these transformations affected the P recovery process.

3.2 P speciation in Fe-enhanced sludge

The P K-edge XANES spectra of sludge samples and references are presented in Figure 2, in which the Fe-P-containing activated sludge mixture from the MBRs is denoted as AS and the sludge after 6-d anaerobic fermentation is denoted as AnS. Each chemical has a unique

"fingerprint" in XANES spectra, which helps deduce qualitative information of the species in unknown samples. The P reference species that bonded with Fe^{III}, such as ferric phosphate and adsorbed-P on HFO (Figure S1), had one pre-edge peak at around 2150 eV, which is attributable to the hybridization of Fe-3d, O-2p, and P-3p orbitals.[32] Most of the sludge samples also had pre-edge peaks, implying Fe^{III}-bonded phosphorus species in the sludge. In the post-edge region, the sludge samples only had two peaks at 2154 and 2170 eV, which are similar to those of ferric phosphate, adsorbed-P, and phytic acid.

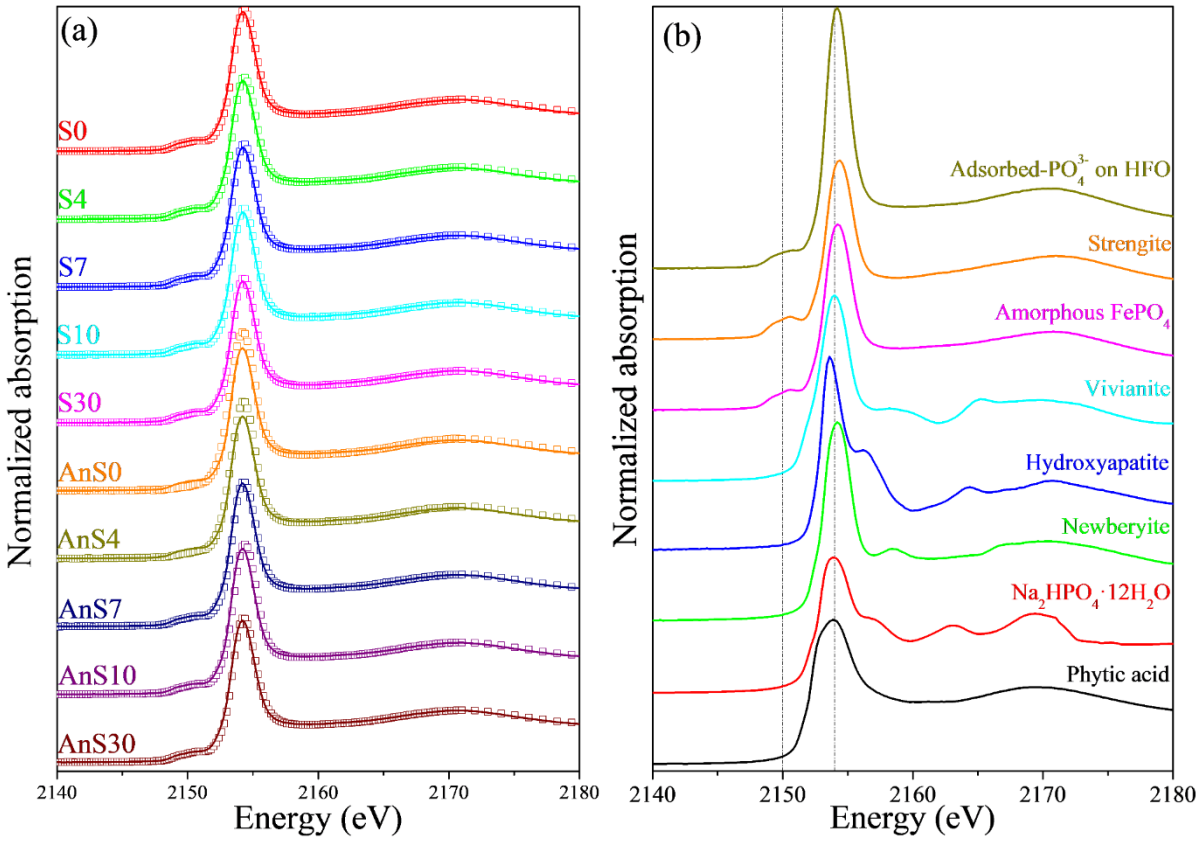

Figure 2. P K-edge XANES analysis of (a) the Fe-P sludge samples with different retention periods in the MBR and (b) the references. For the sludge samples, symbols represent the XANES spectrum data and lines represent the linear combination fitting. S*: Fe-P-containing activated sludge with the corresponding retention periods in the MBR (e.g., S0: 0-d retention sludge), AnS*: anaerobic sludge samples after 6-d fermentation of the sludge with the retention periods indicated (e.g., AnS0: anaerobic samples after 6-d fermentation of the 0-d

retention activated sludge).

To identify possible species in the sludge samples, PCA/TT and LCF were conducted on the P K-edge XANES spectra. The PCA results of the seven sludge samples (Table S2) suggest three principal components with a minimum indicator (IND) of 0.01274 and a cumulative variance of 98.7%. References with a SPOIL value below 3 (as calculated by SIXPack) are normally considered to be reasonably acceptable (i.e., reasonably likely to exist in the sample) and values between 3 and 6 are moderately acceptable.[33] Based on the TT results (Table S3), seven possible reference compounds were further chosen for the LCF analysis,[34] including two reasonably acceptable references with SPOIL values below 3 (amorphous $FePO_4$, adsorbed-P on HFO) and five moderately acceptable references with SPOIL values between 3 and 6 ($Na_2HPO_4 \cdot 12H_2O$, phytic acid, newberyite, vivianite, and hydroxyapatite). Based on the PCA results, the combination of the four most acceptable references was applied for the LCF fitting, and the results with the lowest R-factors were selected as the optimal fitting results.

The XANES LCF analysis results, in combination with the chemical analysis of P species in the sludge samples before and after acidogenic co-fermentation, are given in Figure 3 and Table S4. In the sludge from the aerobic MBRs, the main P species were $FePO_4$ (53-58%) and adsorbed-P (38-43%), which confirmed the two main mechanisms involved in CPR: co-precipitation and adsorption.[35] In coagulation, with the rapid mixing of coagulant $FeCl_3$ into the wastewater, ferric ions reacted with orthophosphate and hydrogen to form ferric phosphate and amorphous ferrihydrite. Fresh ferrihydrite had a very high surface area with abundant reaction sites. During slow-mixing flocculation, the residual orthophosphate was easily adsorbed by the sites of oxygen atoms onto the fresh ferrihydrite surface, leading to more complete P removal from the solution.

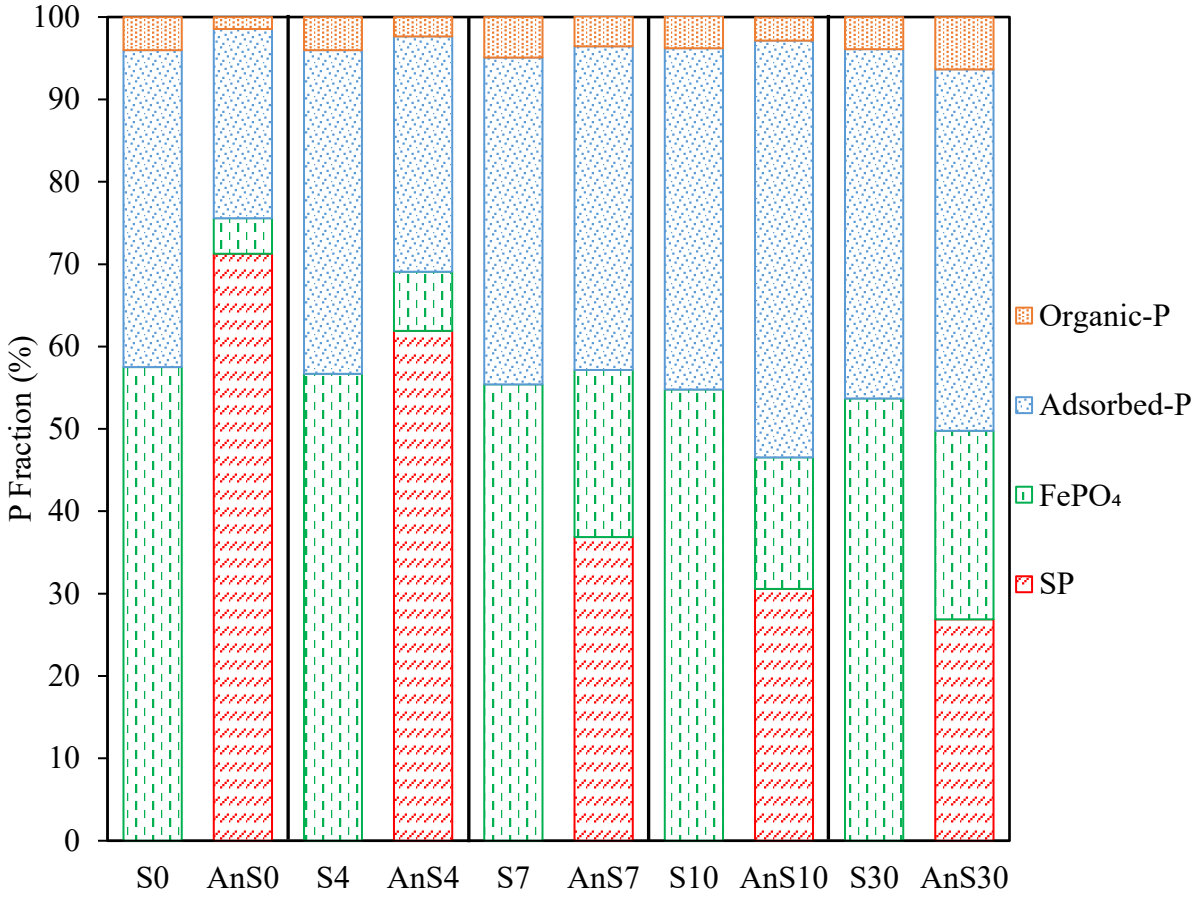

Figure 2. P speciation characterized by the XANES analysis and chemical measurements on the sludge samples with different SRT. SP and TP was determined by the ascorbic acid reduction method.[20] The fraction of solid P was calculated by subtracting SP from TP. Speciation of particulate P was determined by LCF analysis.

After the fermentation, with the reduction of Fe^{III} and dissolution of Fe-P complexes, P was released and dissolved as orthophosphate. Acidogenic fermentation of fresh Fe-containing sludge achieved a P release efficiency of 71.3% at the end of fermentation. With an increase in sludge retention time, the P release efficiency decreased. For retention periods of 7, 10, and 30 d, the P release efficiency from the Fe-P sludge significantly decreased to 36.9%, 30.6%, and 26.9%, respectively, under the same acidogenic co-fermentation conditions. The amount of adsorbed-P in the sludges older than 7 d did not decrease after fermentation, with the fraction

300 of this component being around 40-50% in both activated and fermented sludge. In contrast,
301 the fraction of $FePO_4$ was greatly reduced in all of the fermenters, suggesting that the SP in the
302 supernatant was mainly released from $FePO_4$. It is apparent that $FePO_4$ was reduced to vivianite,
303 which was then dissolved almost completely as orthophosphate and SFe^{II} under the acidic
304 conditions (pH~4.5). Thus, vivianite was not detected in any of the fermented sludge samples.

305 **3.3 Fe speciation in Fe-enhanced sludge**

306 The Fe K-edge XANES spectra of the sludge samples and references are shown in Figure
307 4. In contrast to zero-valent iron and Fe^{II}, the Fe^{III} references had one unique pre-edge peak at
308 7115 eV, which again existed in all samples, suggesting that Fe^{III} was present in the sludge.
309 The E_0 values helped identify the valence states of Fe in different sludge samples. The E_0 of
310 zero-valent iron, Fe^{II}, and Fe^{III} were 7112, 7121, and 7124 eV, respectively. Most of the
311 samples had an E_0 of 7124 eV, indicating that the Fe compounds in the sludge mainly existed
312 in the +3 state.

313 To identify the possible Fe species present in the sludge samples, PCA/TT and LCF were
314 performed on the Fe K-edge XANES spectra. The PCA results on the 10 sludge samples (Table
315 S5) suggested four principal components with a minimum IND of 0.0004 and a cumulative
316 variance of 99.8%. In other words, four main compounds were likely to exist in the sludge
317 samples. Based on the TT results (Table S6), ferrihydrite, goethite, Fe_2O_3, strengite, melanterite,
318 lepidocrocite, and magnetite were moderately acceptable compounds and were selected for the
319 LCF analysis. Based on the PCA results, a combination of the most acceptable four references
320 was applied for the LCF fitting using the function "Fit all combination," and the optimal fitting
321 results were selected as those with the lowest R-factors.

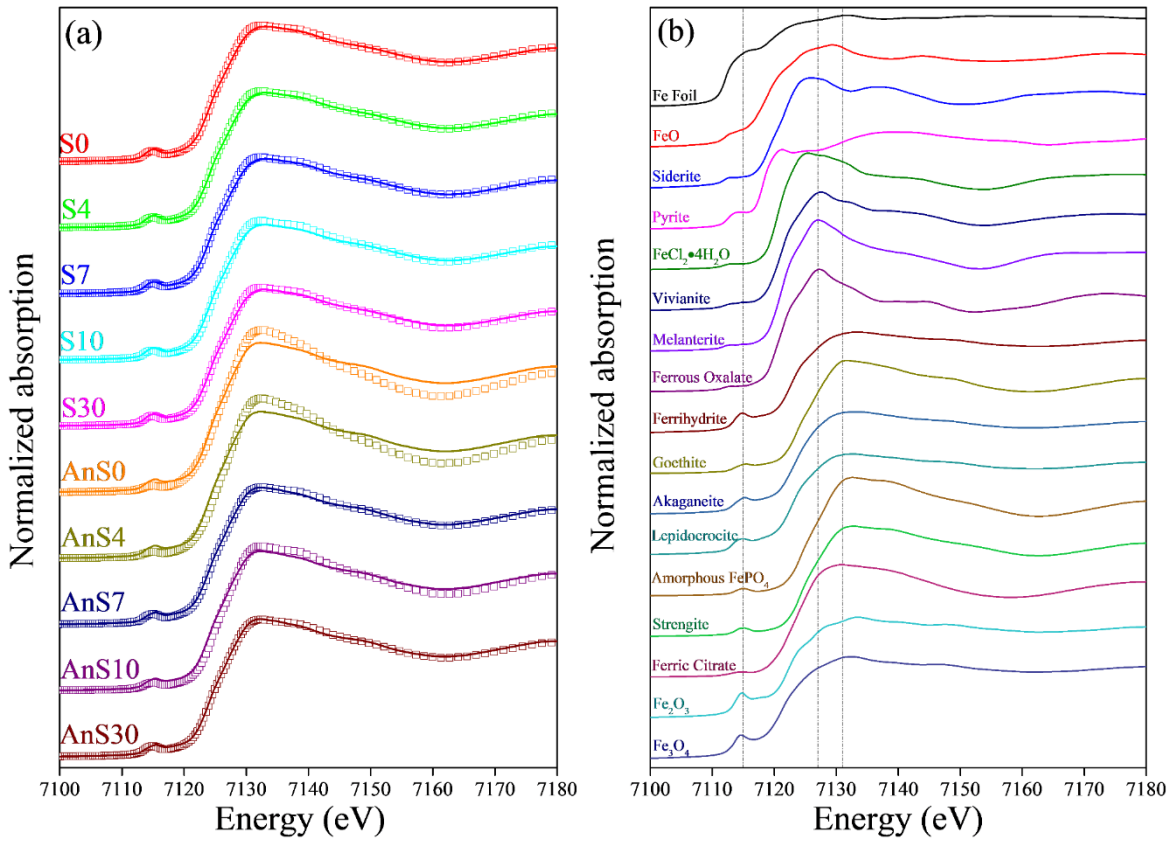

Figure 3. Fe K-edge XANES analysis of (a) the sludge samples with different SRT and (b) the references. For sludge samples, symbols represent the XANES spectrum data and lines represent the linear combination fitting.

The Fe speciation information in the sludge characterized by XANES LCF and chemical measurement is given in Figure 5 and Table S7. For the fresh Fe-P sludge in activated sludge (SRT = 0 d), the main Fe species included $FePO_4$ (31.5%) and ferrihydrite (68.4%), which were formed rapidly by coagulation upon the addition of $FeCl_3$. For the sludge with a retention of 4 d in the MBR, the Fe compositions did not change significantly. After 7 d of retention, the slow crystallization of HFO, with the formation of goethite, was identified in the sludge. From the retention times of 7 to 30 d, the fraction of goethite increased from 5.0% to 9.4%. The appearance of crystalline species is a sign of the loss of reactivity via the HFO aging process.

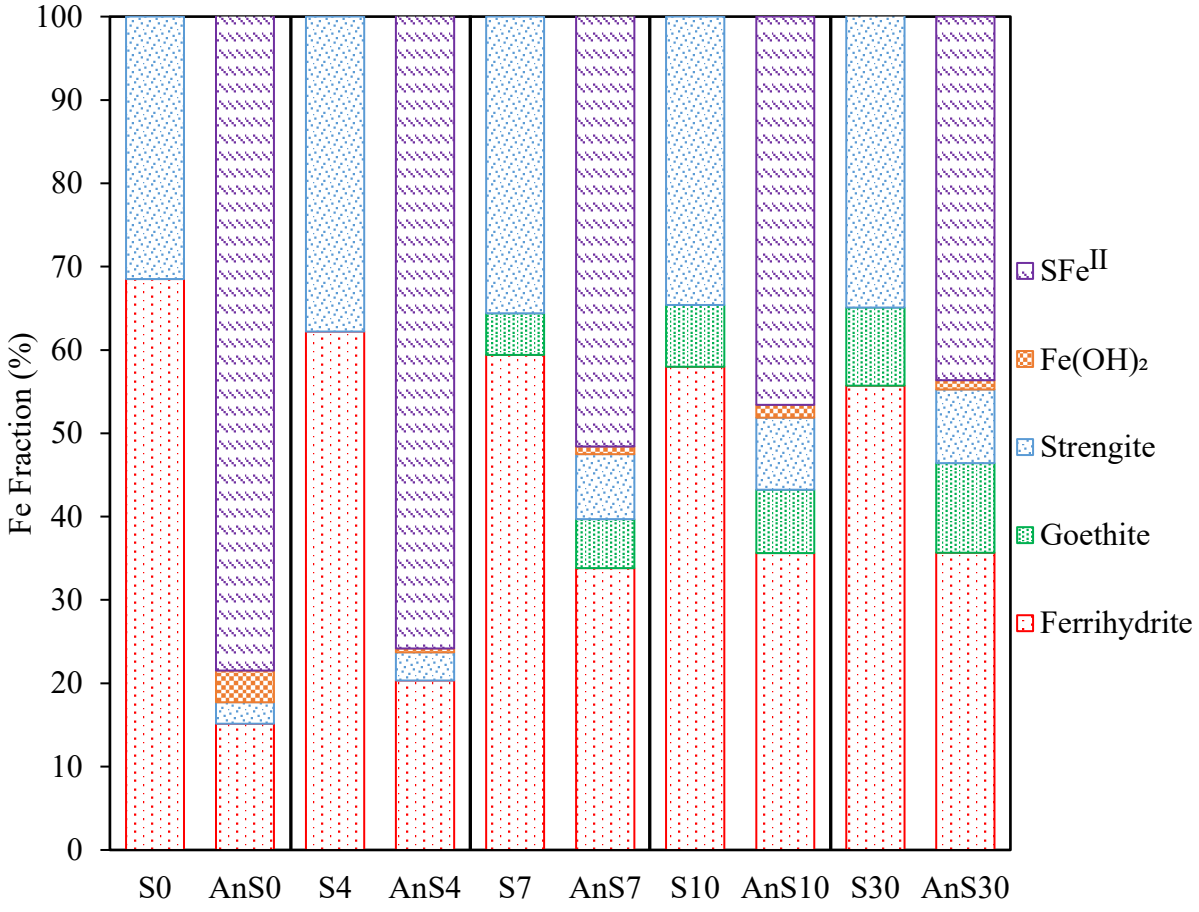

Figure 4. Fe speciation characterized by the chemical measurements and XANES analysis on the sludge samples with different SRT. SFe^{II} and TFe was determined by the phenanthroline method.[20] The fraction of solid Fe was calculated by subtracting SFe^{II} from TFe. Speciation of particulate Fe was determined by LCF analysis.

During the anaerobic sludge co-fermentation, Fe was released from the sludge as soluble ferrous ions. The fresh Fe-P-containing activated sludge showed an excellent release performance, with an increase in SFe^{II} concentration to as high as 667 mg/L after the 6-d fermentation, which amounted to 80% of TFe in the 0-d AS. With the prolonged retention of the Fe-P-containing sludge in the MBRs, the Fe release performance from the sludge during fermentation declined considerably. For the sludge with the retention times of 0 and 4 d in the MBR, the total Fe^{II} fraction after fermentation was 83.8% and 74.5%, respectively. For the

sludge with retention times of 7, 10, and 30 d, the TFe^{II} release fractions were only 52.7%, 48.1%, and 44.7% after the co-fermentation. About 50% of Fe still existed in the solid form in the sludge mixture, which consisted mainly of HFO. The reduction of $FePO_4$ content in the sludge was not affected by aging of the sludge in the MBRs. Even for the 30-d sludge, the fraction of $FePO_4$ in the solid phase significantly decreased from 35.6% to 8.8% after 6-d co-fermentation. $FePO_4$ was found mainly in the amorphous form, which did not undergo polymerization or loss of reactivity during sludge retention in the bioreactors.[36] By acidogenic fermentation, $FePO_4$ was reduced to $Fe_3(PO_4)_2$, which was then completely dissolved in the weak acidic environment. The transformation of HFO appeared to be the main reason for the decrease of Fe solubility in the aged sludge.[37]

3.4 HFO transformation in bioreactors

The transformation of Fe^{III} ions to HFO in wastewater and bioreactors is a multistep process consisting principally of hydrolysis, clustering, aggregation, and crystallization. Numerous intermediate phases of iron compounds arise throughout this process, which might not be directly observable. Computational analysis can provide more information about the details of Fe phase transition during the HFO aging process. The computational results are presented in Figure 6.

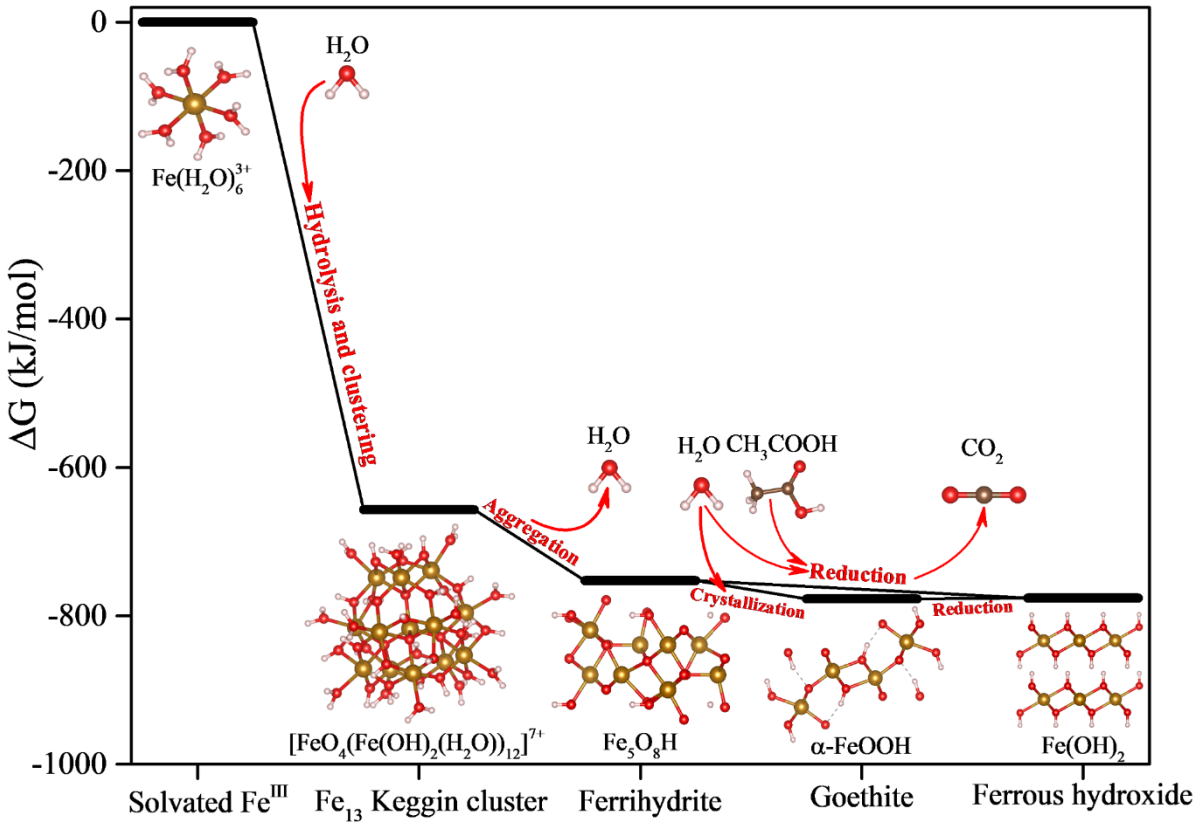

Figure 5. Free-energy diagram for the HFO aging and iron reduction process.

The hydrolysis of Fe^{III} ions took place immediately after $FeCl_3$ addition into the wastewater. Fe^{III} ions in water are usually present as the octahedral, hexahydrated complex $Fe(H_2O)_6^{3+}$.[38] The monomers are rather unstable, which can trigger the formation of Fe^{III} oxyhydroxide clusters from the dimeric oxyhydroxide cluster to give trimeric, tetrameric, or larger stable oligomeric clusters.[39] For calculation of iron clusters composed of high-spin Fe^{III}, the B3LYP/6-31G(d,p) level of theory using the density-based solvation model (SMD) in water was selected.[39] The dominant pathway is shown by the following equations:

$$2Fe(H_2O)_6{}^{3+} \rightarrow Fe_2(H_2O)_8(OH)_2{}^{4+} + 2\,H_3O^+$$

$$\Delta G_1 = 46.02\ \text{kJ/mol} \quad (1)$$

$$Fe_2(H_2O)_8(OH)_2{}^{4+} + Fe(H_2O)_6{}^{3+} \rightarrow Fe_3O(OH)_3(H_2O)_9{}^{4+} + 3H_3O^+$$

$$\Delta G_2 = 97.7\ \text{kJ/mol} \quad (2)$$

$$Fe_3O(OH)_3(H_2O)_9{}^{4+} + 4Fe(H_2O)_6{}^{3+} \rightarrow Fe_7O(OH)_{12}(H_2O)_{12}{}^{7+} + 9H_3O^+ + 3H_2O$$

$$\Delta G_3 = -35.56\ \text{kJ/mol} \quad (3)$$

$$Fe_7O(OH)_{12}(H_2O)_{12}{}^{7+} + 3Fe_2(H_2O)_8(OH)_2{}^{4+} \rightarrow [FeO_4(Fe(OH)_2H_2O)_{12}]^{7+} + 12H_3O^+ + 3H_2O$$

$$\Delta G_4 = -899.56\ \text{kJ/mol} \quad (4)$$

The total reaction free energy of Fe_{13} Keggin cluster formation from monomers was as high as -656.68 kJ/mol, suggesting a rather rapid exothermic reaction in the hydrolysis step. The Fe_{13} Keggin cluster is considered a prenucleation cluster for the formation of aggregated ferrihydrite nanoparticles.[40] The low-molecular-weight hydrated Fe^{III} species interact via olation and oxolation to form ferric species of higher nuclearity, leading to nucleation of ferrihydrite nanoparticles. The structure of ferrihydrite (*P63mc* space group) used in this study was adopted from Pinney et al.[28] based on the single-phase crystal structure proposed by Michel et al.[41] The overall polymerization process can be expressed by the following reaction:

$$\frac{1}{13}Fe_{13}O_{40}H_{41} \rightarrow \frac{1}{5}Fe_5O_8H + \frac{96}{65}H_2O$$

$$\Delta G_5 = -96.06\ \text{kJ/mol} \quad (5)$$

The reaction free energy of this process is -96.06 kJ/mol, which is less than that of hydrolysis, suggesting a spontaneous but slower reaction. Weatherill et al.[40] indicated that when first formed, ferrihydrite particles are of a core-shell structure with a Keggin center surrounded by a water-rich/Fe-depleted shell. The fresh ferrihydrite undergoes a rather complicated aggregation process over days. The smaller hydrated Fe^{III} species (e.g., monomers and dimers) continue to aggregate onto Fe_{13} Keggin clusters, leading to a surface over-saturated with -OH and -OH_2. The fresh ferrihydrite in an unstructured phase is chemically active with a large surface area (typically >290 m^2/g).[40, 42] The saturated -OH and -OH_2 on the surface are exchanged with anions and organic species in water, making the ferrihydrite grow into complex particles. The organics and phosphate in wastewater are mostly removed during this step of the process.

The adsorption of phosphate is achieved via ligand exchange on the ferrihydrite surface to

406 form Fe^{III}-O-P bonds. The adsorption bonds can be monodentate or bidentate.[43] Hiemstra and
407 VanRiemsdijk[44] observed that the dominant adsorbed phosphate species was $H_2PO_4^-$ (more than
408 85%) over the pH range of 3.5-8.0. Adrian et al.[45] calculated that the adsorption of $H_2PO_4^-$ onto
409 HFO clusters was thermodynamically favorable. The adsorption period in chemically enhanced
410 coagulation and flocculation is normally very short (typically less than 30 min). With the
411 consumption of the ferrihydrite adsorption sites by chemical bonding with impurities, the
412 accessibility of the remaining sites decreases, leading to a declining kinetic rate. Hauduc et al.[35]
413 developed a dynamic physicochemical model and predicted that the phosphate adsorption
414 capacity of HFO flocs would be lost in a period from 5 to 30 min.

415 Due to the relatively low surface enthalpy, ferrihydrite is still thought to be less stable than
416 the fully crystalline structures, and its metastable phases transform over time into one of the
417 more stable phases (e.g., goethite, lepidocrocite, or hematite).[46] The structure of ferrihydrite
418 becomes more ordered when the Fe centers become more coordinated, and the bridging bonds
419 are converted from hydroxo-bridges to stronger oxo-bridges, over a period of weeks or longer.
420 This process may occur via dissolution–precipitation reactions or *in situ* rearrangement.[47]
421 Dissolution–precipitation reactions also lead to the phenomenon of particle ripening, where
422 smaller particles preferentially dissolve, leading to the growth of larger particles and a
423 commensurate decrease in reactive surface area.[10] Overall, HFO particles tend to grow or
424 aggregate to form larger particles, potentially leading to a reduction in the amount of surface
425 area that is accessible for reactions. Smith et al.[48] reported a 90% reduction of the specific
426 surface area from fresh HFO to polymerized HFO.

427 In this study, the formation of goethite was identified in the aerobic sludge in the MBRs.
428 The existence of goethite in Fe-containing sludge was also reported in other studies.[14, 37] The
429 conversion of ferrihydrite ($P6_3mc$)[28] to goethite ($pnma$)[25] can be simply expressed as:

430 $$\frac{1}{5}Fe_5O_8H + \frac{2}{5}H_2O \rightarrow \alpha\text{-}FeOOH$$

$$\Delta G_6 = -24.53\ \text{kJ/mol} \quad (6)$$

The free energy of this reaction is only -24.53 kJ/mol, which is smaller than the polymerization reaction and much smaller than hydrolysis, suggesting a slow crystallization process. The transformation of iron species and formation of goethite were indeed observed to be slow in the AS samples from the aerobic bioreactors (Figure 5). Goethite is one of the most thermodynamically stable iron oxyhydroxides.[10] Its crystal structure consists of double chains of edge-shared octahedra that are joined to other double chains by sharing corners and by hydrogen bonds.[49] Goethite may be formed from either Fe^{III} or Fe^{II} systems over a wide pH range.[38] In the Fe^{III} system, goethite can slowly form from freshly prepared ferrihydrite after several days. In the Fe^{II} system, goethite can be an important product of low-temperature oxidation, particularly of iron sulfides. Theoretically, other crystalline phases of HFO might also form under certain conditions. Wu et al.[13] found lepidocrocite formation in chemically enhanced sludge when ferrous sulfate was used in wastewater treatment. It was suggested that lepidocrocite was readily formed via Fe^{II} oxidation at neutral pH.[38] In this study, Fe^{III}-based sludge was retained in the aerobic bioreactors before fermentation; thus, goethite became the dominant crystalline product in the system.

3.5 Impact of HFO aging on acidogenic P recovery

Due to the high reactivity of Fe^{III} clusters and fresh ferrihydrite, the Fe-P bonding is very stable in Fe-facilitated sludge. To extract P from the Fe-P complexes, the polymerized Fe structure needs to be broken and dissolved. Chemical acidification and strong iron reduction have been suggested as effective methods to achieve HFO breakage. Chemical acidification extraction, such as the RecoPhos[50] or Stuttgart processes,[51] has been applied in industry for P recovery. This method uses strong acids to dissolve metal-phosphate compounds from sludge or sludge ash into leachate. However, it not only uses a large amount of expensive and corrosive acids but also causes serious secondary pollution.[7] The APR method is more environmentally

friendly and cost-effective, as the extraction and release of P from the sludge is mainly achieved by microorganisms. In this biological process, microbial iron reduction is a critical step to break the structure of Fe-containing complexes. IRB can utilize soluble organics (mainly acetate and propionate) as electron donors to reduce Fe^{III} to Fe^{II} compounds. The thermodynamic analysis of abiotic HFO reduction by acetate and propionate is as follows.

$$\frac{1}{5}Fe_5O_8H + \frac{1}{8}CH_3COOH + \frac{93}{20}H_2O \rightarrow Fe(OH)_2 + \frac{1}{4}CO_2$$

$$\Delta G_7 = -23.36\ \mathrm{kJ/mol} \quad (7)$$

$$\frac{1}{5}Fe_5O_8H + \frac{1}{14}CH_3CH_2COOH + \frac{164}{35}H_2O \rightarrow Fe(OH)_2 + \frac{3}{14}CO_2$$

$$\Delta G_8 = -23.25\ \mathrm{kJ/mol} \quad (8)$$

$$\alpha\text{–}FeOOH + \frac{1}{8}CH_3COOH + \frac{17}{4}H_2O \rightarrow Fe(OH)_2 + \frac{1}{4}CO_2$$

$$\Delta G_9 = 1.16\ \mathrm{kJ/mol} \quad (9)$$

$$\alpha\text{–}FeOOH + \frac{1}{14}CH_3CH_2COOH + \frac{30}{7}H_2O \rightarrow Fe(OH)_2 + \frac{3}{14}CO_2$$

$$\Delta G_{10} = 1.28\ \mathrm{kJ/mol} \quad (10)$$

Notably, the reaction free energies of acetate- and propionate-induced HFO reduction are relatively small, especially for goethite, which makes them thermodynamically unfavorable. This finding is consistent with the results of Weber et al.[31] who suggested that reduction of goethite required a much lower redox potential (−0.274 V) than that of ferrihydrite (0.014 V). In the acidogenic co-fermentation studied herein, the redox potential was between −0.1 and −0.2 V, which was insufficient for goethite reduction, and instead ferrihydrite and $FePO_4$ were the main iron species that underwent reduction.

The use of microorganisms to facilitate the iron reduction process via enzymatic catalysis is a highly effective strategy. In this reaction, electrons are transferred from an as-yet unidentified terminal Fe reductase[31] in the outer membrane of bacteria to the insoluble Fe^{III} compounds. Some IRB (e.g. *Geobacter* spp.)[52] can come into direct contact with the particles' surfaces and transfer electrons through "nanowires" (conductive extracellular appendages),

some (e.g. *Geothrix* sp.)[53] produce complexing ligands to dissolve solid-phase HFO, while others[54] produce electron shuttles to indirectly transfer electrons to Fe^{III} compounds. In all cases, contact sites are necessary. With a sufficient amount of accessible surface area, the Fe^{III} can be rapidly reduced and its polymerized structure broken and dissolved. In this study, more than 80% of Fe^{II} ions were released from the fresh Fe-P-containing sludge after only 3 d of fermentation. However, when the amount of active sites was greatly reduced via the prolonged sludge retention and HFO aging process, the iron reduction potential decreased significantly. When the retention time of the Fe-P sludge in the MBR was more than 10 d, only 40-50% of Fe^{III} was reduced and dissolved by sludge fermentation, corresponding to a much-reduced P release. Moreover, a small fraction of $FePO_4$ was found to remain in the fermented sludge. It has been reported that orthophosphate and Fe can precipitate on the surface of iron oxide particles to form three-dimensional $FePO_4$ minerals (in contrast, P adsorbs as a two-dimensional monolayer).[55] This recalcitrant $FePO_4$ in the sludge was buried in aggregated polymers during the growth of HFO particles, which had a limited accessible surface area for iron reduction and P mobilization. In conclusion, owing to the condensed structure of aged HFO and the loss of its reactivity by crystallization, the HFO aging process is a critical limiting factor that affects the performance of APR from the Fe-based sludge.

3.6 Environmental implications

In this study, APR was proven to be an effective and environmentally friendly method for P extraction and recovery from Fe-based CPR sludge. However, the performance and efficiency of APR via co-fermentation from Fe-P-containing sludge is affected by the retention and aging of the sludge in the aerobic bioreactors. The decreasing microbial iron reduction potential of Fe-based sludge after aging was found to be the main reason for this phenomenon. In further investigation, XANES detection showed that amorphous Fe-P complexes (e.g., $FePO_4$ and fresh ferrihydrite) in sludge were readily mobilized via microbial iron reduction

during acidogenic fermentation, while aggregated and crystalline HFO (e.g., aged ferrihydrite and goethite) were less susceptible to biological reduction and mobilization. Thus, it is suggested that fresh Fe-P-containing sludge is much more amenable than aged sludge to effective P recovery via acidogenic co-fermentation. In other words, as far as P recovery from the sludge is concerned, aging of the P-containing sludge should be minimized in wastewater treatment systems. In conclusion, the study provided important insights into the transformation of Fe-P complexes in wastewater treatment and its effect on APR. The findings and related mechanisms will help researchers to improve the process and develop new strategies for effective P removal and recovery from wastewater.

Acknowledgments

We gratefully acknowledge the funding for this research provided by grants 51678333 and 51908316 from the National Natural Science Foundation of China, grant JCYJ20180508152004176 from the Shenzhen Municipal Science and Technology Innovation Council, and grants 17204914 and T21-711/16R from the Research Grants Council (RGC) of Hong Kong. The XANES beam time was granted by beamline BL16A1 at the NSRRC of Taiwan. We thank Dr. Ting-shan Chan and Mr. Shih-Tien Tang of the NSRRC for their help in the collection and analysis of spectra.

The authors declare no competing financial interest.

Supporting Information Available

The Supporting Information contains 7 tables and 2 figures. This material is available free of charge via the Internet at http://pubs.acs.org.

Literature Cited

(1) Cordell, D.; Drangert, J.-O.; White, S., The story of phosphorus: global food security and food for thought. *Global Environmental Change* **2009,** *19*, (2), 292-305.

(2) MEE, *Environmental quality standards for surface water (GB3838-2002), Ministry of Ecology and Enviornment, PR China*, Environmental Science Press: Beijing, 2003.

(3) Liu, W.-j.; Hu, Z.-r.; Walker, R.; Dold, P., Enhanced nutrient removal MBR system with chemical addition for low effluent TP. *Water Science & Technology* **2011,** *64*, (6), 1298-1306.

(4) Yang, X. L.; Song, H. L.; Chen, M.; Cheng, B., Characterizing membrane foulants in MBR with addition of polyferric chloride to enhance phosphorus removal. *Bioresource Technology* **2011,** *102*, (20), 9490-9496.

(5) Zhang, Z. H.; Wang, Y.; Leslie, G. L.; Waite, T. D., Effect of ferric and ferrous iron addition on phosphorus removal and fouling in submerged membrane bioreactors. *Water Research* **2015,** *69*, 210-222.

(6) BMUB. New sewage sludge ordinance passed the German cabinet. http://phosphorusplatform.eu/scope-in-print/news/1395-new-sewage-sludge-ordinance-passed (18 Oct 2019).

(7) Petzet, S.; Peplinski, B.; Cornel, P., On wet chemical phosphorus recovery from sewage sludge ash by acidic or alkaline leaching and an optimized combination of both. *Water Research* **2012,** *46*, (12), 3769-3780.

(8) de-Bashan, L. E.; Bashan, Y., Recent advances in removing phosphorus from wastewater and its future use as fertilizer (1997–2003). *Water Research* **2004,** *38*, (19), 4222-4246.

(9) Li, R. H.; Wang, X. M.; Li, X. Y., A membrane bioreactor with iron dosing and acidogenic co-fermentation for enhanced phosphorus removal and recovery in wastewater treatment. *Water Research* **2018,** *129*, 402-412.

(10) Cornell, R. M.; Schwertmann, U., *The Iron Oxides: Structure, Properties, Reactions, Occurrences and Uses*, Wiley: New York, 2003.

(11) Wilfert, P.; Kumar, P. S.; Korving, L.; Witkamp, G.-J.; van Loosdrecht, M. C., The relevance of phosphorus and iron chemistry to the recovery of phosphorus from wastewater: a review. *Environmental Science & Technology* **2015,** *49*, (16), 9400-9414.

(12) Wang, X. M.; Waite, T. D., Iron speciation and iron species transformation in activated

562 sludge membrane bioreactors. *Water Research* **2010,** *44*, (11), 3511-3521.
563 (13) Wu, H.; Ikeda Ohno, A.; Wang, Y.; Waite, T. D., Iron and phosphorus speciation in Fe-
564 conditioned membrane bioreactor activated sludge. *Water Research* **2015,** *76*, 213-226.
565 (14) Georgaki, I.; Dudeney, A. W. L.; Monhemius, A. J., Characterisation of iron-rich sludge:
566 correlations between reactivity, density and structure. *Minerals Engineering* **2004,** *17*, (2),
567 305-316.
568 (15) Bonneville, S.; Behrends, T.; Van Cappellen, P.; Hyacinthe, C.; Roling, W. F. M.,
569 Reduction of Fe(III) colloids by Shewanella putrefaciens: A kinetic model. *Geochimica et*
570 *Cosmochimica Acta* **2006,** *70*, (23), 5842-5854.
571 (16) Li, R. H.; Wang, W. J.; Li, B.; Zhang, J. Y.; Liu, J.; Zhang, G. J.; Guo, X. C.; Zhang, X.
572 H.; Li, X. Y., Acidogenic phosphorus recovery from the wastewater sludge of the
573 membrane bioreactor systems with different iron-dosing modes. *Bioresource Technology*
574 **2019,** *280*, 360-370.
575 (17) Ressler, T.; Wong, J.; Roos, J.; Smith, I. L., Quantitative speciation of Mn-bearing
576 particulates emitted from autos burning (methylcyclopentadienyl) manganese tricarbonyl-
577 added gasolines using XANES spectroscopy. *Environmental Science & Technology* **2000,**
578 *34*, (6), 950-958.
579 (18) Webb, S. M., SIXpack: a graphical user interface for XAS analysis using IFEFFIT.
580 *Physica Scripta* **2005,** *2005*, (T115), 1011.
581 (19) Ravel, B.; Newville, M., ATHENA, ARTEMIS, HEPHAESTUS: data analysis for X-ray
582 absorption spectroscopy using IFEFFIT. *Journal of Synchrotron Radiation* **2005,** *12*, 537-
583 541.
584 (20) APHA, *Standard Methods for Examination of Water and Wastewater, 22nd Edition*,
585 American Public Health Association, American Water Work Association, Water
586 Environment Federation: Washington DC, 1998.
587 (21) Kresse, G.; Furthmüller, J., Efficiency of ab-initio total energy calculations for metals and
588 semiconductors using a plane-wave basis set. *Comp.mat.er.sci* **1996,** *6*, (1), 15-50.
589 (22) Perdew, J. P.; Burke, K.; Ernzerhof, M., Generalized gradient approximation made simple.
590 *J Physical Review Letters* **1996,** *77*, (18), 3865-3868.
591 (23) Fuente, S. A.; Belelli, P. G.; Castellani, N. J.; Avena, M. J. M. C., LDA + U and GGA + U
592 studies of Al-rich and bulk goethite (α-FeOOH). *Materials Chemistry Physics* **2013,** *137*,
593 (3), 1012-1020.
594 (24) Klyukin, K.; Rosso, K. M.; Alexandrov, V., Iron dissolution from goethite (α-FeOOH)
595 surfaces in water by Ab initio enhanced free-energy simulations. *Journal of Physical*

596 *Chemistry C* **2018,** *122*, (28), 16086-16091.
597 (25) Zepeda-Alarcon, E.; Nakotte, H.; Gualtieri, A. F.; King, G.; Page, K.; Vogel, S. C.; Wang,
598 H. W.; Wenk, H. R., Magnetic and nuclear structure of goethite (α-FeOOH): A neutron
599 diffraction study. *Journal of Applied Crystallography* **2014,** *47*, (6), 1983–1991.
600 (26) Wang, V.; Xu, N., *VASPKIT: A Pre- and Post-Processing Program for the VASP Code*,
601 2019.
602 (27) Otte, K.; Schmahl, W. W.; Pentcheva, R., Density functional theory study of water
603 adsorption on FeOOH surfaces. *Surface Science* **2012,** *606*, (21-22), 1623-1632.
604 (28) Pinney, N.; Kubicki, J. D.; Middlemiss, D. S.; Grey, C. P.; Morgan, D., Density functional
605 theory study of ferrihydrite and related Fe-oxyhydroxides. *Chemistry of Materials* **2015,**
606 *21*, (24), 5727-5742.
607 (29) Lin, L.; Li, R. H.; Yang, Z. Y.; Li, X. Y., Effect of coagulant on acidogenic fermentation
608 of sludge from enhanced primary sedimentation for resource recovery: Comparison
609 between FeCl3 and PACl. *Chemical Engineering Journal* **2017,** *325*, 681-689.
610 (30) Li, R. H.; Li, X. Y., Recovery of phosphorus and volatile fatty acids from wastewater and
611 food waste with an iron-flocculation sequencing batch reactor and acidogenic co-
612 fermentation. *Bioresource Technology* **2017,** *245*, (Part A), 615-624.
613 (31) Weber, K. A.; Achenbach, L. A.; Coates, J. D., Microorganisms pumping iron: anaerobic
614 microbial iron oxidation and reduction. *Nature Reviews: Microbiology* **2006,** *4*, (10), 752-
615 764.
616 (32) Xiong, W.; Peng, J.; Hu, Y., Use of X-ray absorption near edge structure (XANES) to
617 identify physisorption and chemisorption of phosphate onto ferrihydrite-modified
618 diatomite. *Journal of Colloid and Interface Science* **2012,** *368*, (1), 528-532.
619 (33) Malinowski, E. R., *Factor Analysis in Chemistry, 3rd Edition*, Wiley: New York, 2002.
620 (34) Cui, J.; Jing, C.; Che, D.; Zhang, J.; Duan, S., Groundwater arsenic removal by coagulation
621 using ferric(III) sulfate and polyferric sulfate: A comparative and mechanistic study.
622 *Journal of Environmental Sciences* **2015,** *32*, 42-53.
623 (35) Hauduc, H.; Takács, I.; Smith, S.; Szabo, A.; Murthy, S.; Daigger, G. T.; Spérandio, M.,
624 A dynamic physicochemical model for chemical phosphorus removal. *Water Research*
625 **2015,** *73*, 157-170.
626 (36) Luedecke, C.; Hermanowicz, S. W.; Jenkins, D., Precipitation of ferric phosphate in
627 activated sludge: a chemical model and its verification. *Water Science and Technology*
628 **1989,** *21*, (4-5), 325-337.

(37) Li, R. H.; Cui, J. L.; Li, X. D.; Li, X. Y., Phosphorus removal and recovery from wastewater using Fe-dosing bioreactor and cofermentation: Investigation by X-ray absorption near-edge structure spectroscopy. *Environmental Science & Technology* **2018,** *52*, (24), 14119-14128.

(38) Schwertmann, U.; Cornell, R. M., *Iron Oxides in the Laboratory: Preparation and Characterization*, Wiley‐VCH: Weinheim, 2000.

(39) Das, B., Theoretical study of small iron–oxyhydroxide clusters and formation of ferrihydrite. *The Journal of Physical Chemistry A* **2018,** *122*, (2), 652-661.

(40) Weatherill, J. S.; Morris, K.; Bots, P.; Stawski, T. M.; Janssen, A.; Abrahamsen, L.; Blackham, R.; Shaw, S., Ferrihydrite formation: The role of Fe13 Keggin clusters. *Environmental Science & Technology* **2016,** *50*, (17), 9333-9342.

(41) Michel, F. M.; Ehm, L.; Antao, S. M.; Lee, P. L.; Chupas, P. J.; Liu, G.; Strongin, D. R.; Schoonen, M. A. A.; Phillips, B. L.; Parise, J. B., The structure of ferrihydrite, a nanocrystalline material. *Science* **2007,** *316*, (5832), 1726-1729.

(42) Jambor, J. L.; Dutrizac, J. E., Occurrence and constitution of natural and synthetic ferrihydrite, a widespread iron oxyhydroxide. *Chemical Reviews* **1998,** *98*, (7), 2549-2585.

(43) Kim, J.; Li, W.; Philips, B. L.; Grey, C. P., Phosphate adsorption on the iron oxyhydroxides goethite (α-FeOOH), akaganeite (β-FeOOH), and lepidocrocite (γ-FeOOH): A 31P NMR Study. *Energy Environmental Science* **2011,** *4*, (10), 4298-4305.

(44) Hiemstra, T.; VanRiemsdijk, W. H., A surface structural approach to ion adsorption: The charge distribution (CD) model. *Journal of Colloid and Interface Science* **1996,** *179*, (2), 488-508.

(45) Adamescu, A.; Hamilton, I. P.; Al-Abadleh, H. A., Thermodynamics of dimethylarsinic acid and arsenate interactions with hydrated iron-(oxyhydr)oxide clusters: DFT calculations. *Environmental Science & Technology* **2011,** *45*, (24), 10438-10444.

(46) Navrotsky, A.; Mazeina, L.; Majzlan, J., Size-driven structural and thermodynamic complexity in iron oxides. *Science* **2008,** *319*, (5870), 1635.

(47) Jolivet, J. P.; Chaneac, C.; Tronc, E., Iron oxide chemistry. From molecular clusters to extended solid networks. *Chemical Communications* **2004**, (5), 481-487.

(48) Smith, S.; Takacs, I.; Murthy, S.; Daigger, G. T.; Szabo, A., Phosphate complexation model and its implications for chemical phosphorus removal. *Water Environment Research* **2008,** *80*, (5), 428-438.

(49) Hillel, D.; Hatfield, J. L., *Encyclopedia of Soils in the Environment*, Elsevier: Oxford, 2005.

(50) Weigand, H.; Bertau, M.; Hübner, W.; Bohndick, F.; Bruckert, A., RecoPhos: Full-scale fertilizer production from sewage sludge ash. *Waste Management* **2013,** *33*, (3), 540-544.
(51) Egle, L.; Rechberger, H.; Krampe, J.; Zessner, M., Phosphorus recovery from municipal wastewater: An integrated comparative technological, environmental and economic assessment of P recovery technologies. *Science of the Total Environment* **2016,** *571*, 522-542.
(52) Nevin, K. P.; Lovley, D. R., Lack of production of electron-shuttling compounds or solubilization of Fe(III) during reduction of insoluble Fe(III) oxide by Geobacter metallireducens. *Applied and Environmental Microbiology* **2000,** *66*, (5), 2248-2251.
(53) Lovley, D. R.; Coates, J. D.; BluntHarris, E. L.; Phillips, E. J. P.; Woodward, J. C., Humic substances as electron acceptors for microbial respiration. *Nature* **1996,** *382*, (6590), 445-448.
(54) Newman, D. K.; Kolter, R., A role for excreted quinones in extracellular electron transfer. *Nature* **2000,** *405*, (6782), 94-97.
(55) Sparks, D. L., Sorption Phenomena on Soils. In *Environmental Soil Chemistry, 2nd Edition*, Sparks, D. L., Ed. Academic Press: Burlington, 2003; pp 133-186.